Electromagnetic Guiding of Vertical Transportation Vehicles: Experimental Evaluation

Rüdiger Appunn, Benedikt Schmülling, and Kay Hameyer, *Senior Member, IEEE*

***Abstract*—This paper describes the design of an electromagnetic elevator guiding system. One challenge of this design is the overdetermination of the mechanical system due to its high number of adjustment variables. Force decoupling, transformation from local to global quantities, and simulation results of the entire system are presented. In contrast to former works, a new elevator test bench for the evaluation of the simulation results is introduced. Measurement results validate the design process of both the electromagnetic actuators and feedback control.**

***Index Terms*—Electromagnetic actuator, elevator test bench, force decoupling, guideway transportation, linear guiding system, magnetic levitation (maglev), mechatronics, modeling, motion control, simulation.**

NOMENCLATURE

α, β, and γ	Rotatory degrees of freedom (DOFs).
δ_{sensor}	Array of observed air gaps.
δ	Air-gap length.
$\mathbf{A_x}$	System matrix.
$\mathbf{B_x}$	Input matrix.
$\mathbf{C_x}$	Output matrix.
$\mathbf{D_x}$	Feedback matrix.
$\mathbf{f_{ext}}$	Local forces.
$\mathbf{f_{local}}$	External forces.
$\mathbf{K_x}$	Control matrix.
$\mathbf{M}$	Symmetrical mass matrix.
$\mathbf{q}$	Position vector.
$\mathbf{T_F}$	Transformation matrix (forces).
$\mathbf{T}$	Transformation matrix (air gaps).
μ_0	Permeability of the vacuum.
ω	Angular frequency.
$\Phi_{\mathrm{El1,El2}}$	Electrically excited flux.
Φ_{PM}	Permanent magnet flux.
Θ	Magnetomotive force (MMF).
$\Theta_{x0,\Theta 0}$, U_0	Linearization factors (MMFs).
$\tilde{\Theta}_x$	Global MMF in the x-direction.
A	Cross section of the air gap.
B_r	Remanence of the permanent magnet.
$F_{\delta x,\Theta x}$	Linearization factors (forces).
$F_{x1,x2,x3,x4}$	Forces in the x-direction.
$F_{y1,y2}$	Forces in the y-direction.
H_C	Coercivity of the permanent magnet.
h_{pm}	Magnet height.
$I_{x,y,z}$	Moments of inertia of the elevator car.
m	Mass of the elevator car.
R_δ	Reluctance of the air gap.
R_{PM}	Reluctance of the permanent magnet.
w	Number of windings.
x, y, z	Translatory DOFs.
$\mathbf{q_0}$	Working point.
A/D	Analog/digital.
b	Horizontal distance between two three-armed actuators (TAAs).
D/A	Digital/analog.
dc	Direct current.
h	Vertical distance between two TAAs.

I. INTRODUCTION

MORE and more high-rise buildings are being built nowadays, particularly in Asia. Examples are the Taipei Financial Center in Taiwan, the Petronas Towers in Malaysia, and the Burj Dubai in the United Arab Emirates, which is still under construction. Designing elevator systems for such buildings is a challenging task. The height and the number of floors increase year after year, and conventional elevators with mechanical guiding reach their limits. Modern designs advocate the use of linear motors instead of a rope for the elevator car's propulsion as well [1]. Recently, linear switched reluctance motor drives are in focus of research [2]–[4]. The benefits of linear drives are a higher dynamic behavior and the opportunity to equip elevator shafts with more than one elevator car. Batelaan [5] proposes an "individual pole excitation linear motor" to operate many vehicles on the same guideway. An improvement of the operational behavior of such elevator systems can be achieved by using wear- and lubricant-free electromagnetic guides, instead of slide or roller guides. Electromagnetic actuators are used in a wide field of applications: Yang and Huang [6] have proposed an actuator for an axial blood pump, an electromagnetic vibratory actuator for material conveying is shown by Despotovic and Stojiljkovic [7], or a spherical actuator based on magnetic-dipole-moment principle introduced by Lim *et al.* [8]. Therefore, a solution for the design of both the electromagnets and the feedback control of an elevator guiding system is presented in this paper.

Manuscript received February 27, 2009; revised September 9, 2009. First published September 22, 2009; current version published December 11, 2009.

The authors are with the Institute of Electrical Machines, RWTH Aachen University, 52062 Aachen, Germany (e-mail: ruediger.appunn@iem.rwth-aachen.de).

Color versions of one or more of the figures in this paper are available online at http://ieeexplore.ieee.org.

Digital Object Identifier 10.1109/TIE.2009.2032432

0278-0046/$26.00 © 2010 IEEE

Authorized licensed use limited to: RWTH AACHEN. Downloaded on January 18, 2010 at 10:53 from IEEE Xplore. Restrictions apply.

One benefit of electromagnetic guideways is their wear-free operation. In addition, these guideways have no consumption of lubricants, which is a further advantage compared to mechanical guideways. Due to the frictionless operation, the elevator can be operated at a higher speed than the conventional systems. Only the energy supply for actuators and electronics of the elevator car has to be realized via sliding contacts. Even the need of physical contacts becomes redundant by using an inductive power transfer system, e.g., similar to automotive systems [9], [10]. However, the main advantage of electromagnetic bearing is the possibility to control the ride comfort by adjusting the damping rate of the guiding system. The ride comfort depends on vibration and noise caused by misalignment and misconnection of the guide rail segments. Chen *et al.* [11] have proposed an alternative approach evaluating the effect of eddy currents on diamagnetic bearings to adjust the damping for vibration control of a levitated body. This topic and the opportunity to improve the convenience are presented in further literature, for example, in [12]. The active control of the damping rate requires a closed-loop system.

Manufacturing tolerances and the need to keep the elevator car within a narrow range around the central position lead to high demands on the guiding topology and the control system. The quality of the position sensor signals has to be kept as high as possible, and the ride control characteristics of the elevator car have to be very smooth and convenient to achieve a high ride comfort. The elevator car is assumed to be a rigid body. It is fixed in one DOF by its propulsion device (a rope or a linear drive, for example). This is the DOF in vertical z-direction. The other five DOFs are the translatory movements in x- and y-directions and the rotary movements α, β, and γ around the axes of a Cartesian coordinate system located at the center of gravity of the elevator car. A DOF control system is created to stabilize the elevator car. The maglev system presented by Chen *et al.* [13] or the motion control for robotic systems introduced by Tsuji *et al.* [14] is based on DOF control, too. Magnetically levitated vehicles for horizontal applications possess an offset force, the gravity, which has to be compensated. However, the displacement of the elevator car from its designated position can occur in any direction. For this purpose, an arrangement of electromagnets, which are able to balance displacements in all directions and angles, is required.

II. Guiding Topology

An important component of the guideway is the so-called guiding shoe, which transmits disturbance forces from the elevator car to the guide rail. Conventional guiding shoes are constructed using rollers or slideways. The proposed electromagnetic alternative presented is TAA [12]. The TAA is an electromagnetic actuator that is able to excite three pulling forces. This is a significant improvement with respect to conventional u-shaped actuators [15], which generate a pulling force in one direction only. Therefore, one TAA replaces three u-actuators. A further actuator is the magnet module presented in [16], which controls one complete DOF, i.e., producing a force in one direction (positive and negative). Nevertheless, the TAA controls one and a half DOF. Therewith, two TAAs substitute three magnet modules.

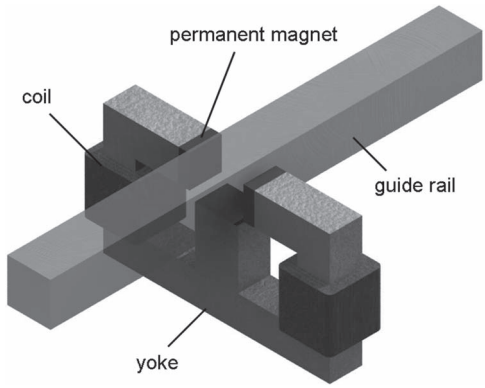

Fig. 1. TAA on a guide rail.

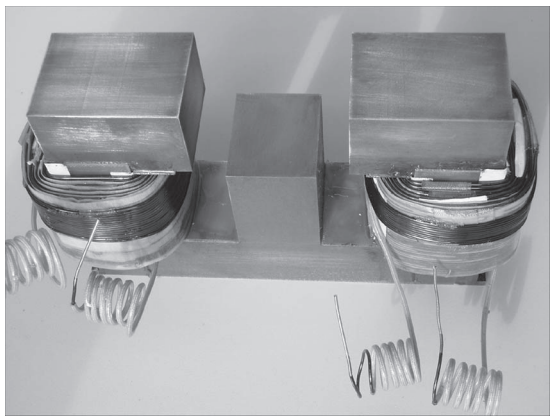

Fig. 2. Prototype of a TAA.

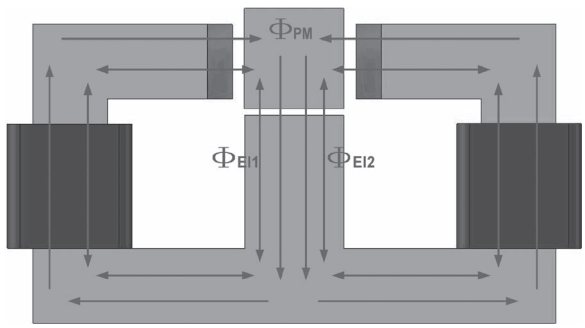

Fig. 3. Superposed fluxes in a TAA's cross section.

Fig. 1 shows the schematic of a TAA, and Fig. 2 shows a prototype of it (in the figure without permanent magnets). It consists of a three-armed iron yoke, mounted with permanent magnets on the outer pole surfaces, and coils around the lateral arms. The operation of this actuator is based on the superposition of a permanent magnet flux Φ_{PM} with electrically excited fluxes Φ_{El1} and Φ_{El2}. The cross section and the fluxes in the actuator are shown in Fig. 3. The analytical calculation of the actuator's magnetic fluxes is based on the method of the magnetic equivalent circuit (MEC), which works similarly to an electrical equivalent network. At first, sources and magnetic resistances (reluctances) are determined. As a first approximation, the reluctance of the iron yokes and the guide rail is

Authorized licensed use limited to: RWTH AACHEN. Downloaded on January 18, 2010 at 10:53 from IEEE Xplore. Restrictions apply.

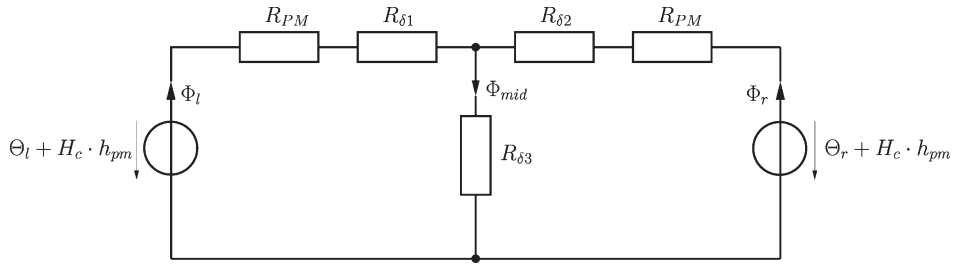

Fig. 4. Magnetic equivalent circuit of the TAA.

neglected due to their high permeability compared to that of the air gaps. The reluctances of air gap R_δ and permanent magnet R_{PM} are determined as follows:

$$R_\delta = \frac{\delta}{\mu_0 A} \tag{1}$$

$$R_{\mathrm{PM}} = \frac{h_{\mathrm{pm}} H_c}{B_r A} \tag{2}$$

where A is the cross section of the air gap, μ_0 is the permeability of the vacuum, H_c is the coercivity, and B_r is the remanence of the permanent magnet. δ and h_{pm} are the heights of air gap and magnet, respectively. The sources in the MEC are the two permanent magnets and the two coils. The MMF of one coil is defined as $\Theta = w \cdot i$, and the MMF of one magnet is equal to $H_c \cdot h_{\mathrm{pm}}$. With this information, the resulting equivalent network of the magnetic circuit can be established (Fig. 4).

During operation, the three guiding forces occur in the air gaps of the actuator/guide rail system. They depend on the air-gap fluxes Φ_r, Φ_l, and Φ_y. From the MEC, it can be seen that each force depends on all air gaps and all MMFs. Thus, a mathematical decoupling of the forces is required to design an adequate control system.

The actuators are mounted on the opposite edges of the roof and floor of the elevator car, i.e., four TAAs are mounted on one car. In combination with two guide rails located on the opposite walls of the elevator shaft, the complete guiding system is formed (Fig. 5). Altogether, the four TAAs produce 12 pulling forces, organized in pairs along six action lines. Hence, a total of six forces remain to control the position of the elevator car, i.e., to control the five DOFs (x, y, α, β, and γ). These forces are shown in Fig. 6. On the left-hand side, the 12 individual forces are presented. On the right-hand side, the forces acting on the same line are merged into the six control forces F_{x1}, F_{x2}, F_{x3}, F_{x4}, F_{y1}, and F_{y2}. Due to the fact that the three forces of each TAA are driven by two coils, eight linearly independent current variables are available for adjusting them. Therefore, the guiding of an elevator car by means of TAAs necessitates a feedback control of an overdetermined system.

The implementation of a state-space controller requires a linear time-invariant system. However, the pulling force F between an actuator arm and the guide rail depends quadratically on the magnetic flux. Thus, the guiding system is nonlinear. Nonetheless, to control the system, a mathematical linearization of all forces is accomplished [17].

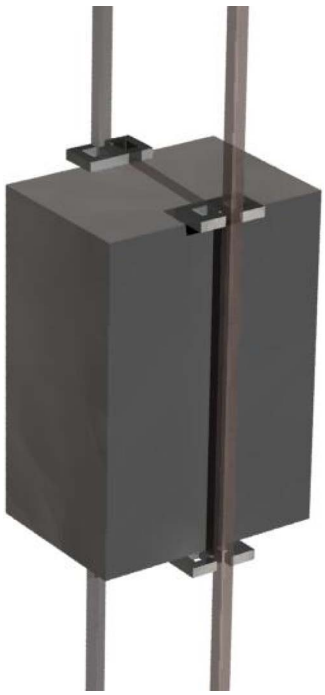

Fig. 5. Elevator car guided by four TAAs.

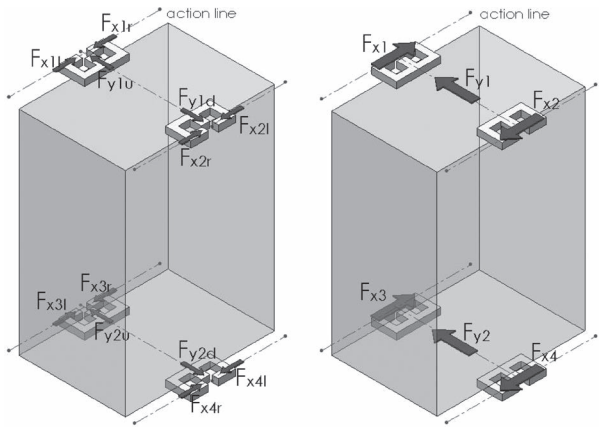

Fig. 6. (Left) Individual forces and (right) superposed forces of all TAAs.

III. State-Space Model

Elevator cars for passenger transportation have a typical rated load of 630 kg. It is supposed to behave like a rigid body. The dynamic model consists of the mechanical

Authorized licensed use limited to: RWTH AACHEN. Downloaded on January 18, 2010 at 10:53 from IEEE Xplore. Restrictions apply.

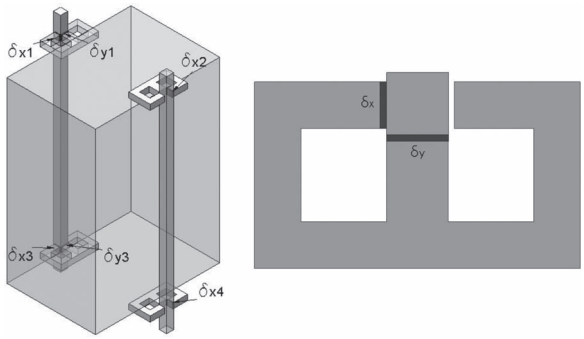

Fig. 7. Observed air gaps.

equations of the elevator car and the electromagnetic equations of the four actuators. One defines the position vector of the car as

$$\mathbf{q} = (\, x \quad y \quad \alpha \quad \beta \quad \gamma \,)^{\mathrm{T}}. \tag{3}$$

The forces of the actuators depend on the air-gap heights, which have to be calculated from the vehicle position. Reciprocally, the forces of the actuators have to be converted into the elevator car coordinates. Therefore, a mapping between $\mathbf{q}$ and the TAA variables is established [17].

A. Transformation of Local Quantities

The components of $\mathbf{q}$ are global quantities. However, the measured quantities on the elevator car are the local air gaps. Thus, a transformation has to be performed to control $\mathbf{q}$ with the aid of the sensor signals. In Fig. 7, the positioning of six air-gap sensors is presented. It can be seen that six air gaps are observed, although there are only five DOFs. Here, for the transformation to the global quantities, only five air-gap sensor signals are required in principle. However, due to manufacturing tolerances, the calculation of the spatial position is easier with additional sensors. The vector of the observed air gaps is

$$\boldsymbol{\delta}_{\mathbf{sensor}} = (\, \delta_{x1} \quad \delta_{y1} \quad \delta_{x2} \quad \delta_{x3} \quad \delta_{y3} \quad \delta_{x4} \,)^{\mathrm{T}}. \tag{4}$$

For instance, the translatory movement in the x-direction is deduced from the signed average of four air-gap heights

$$x = \frac{1}{4}(\Delta\delta_{x1} - \Delta\delta_{x2} + \Delta\delta_{x3} - \Delta\delta_{x4}). \tag{5}$$

The signs of opposite actuators are different. The translatory movement in the y-direction is calculated similarly, but only two air gaps are available

$$y = \frac{1}{2}(\Delta\delta_{y1} + \Delta\delta_{y3}). \tag{6}$$

The angular positions are deduced from the local quantities by means of trigonometrical relationships. For α,

$$\alpha = \arctan\left(\frac{-\Delta\delta_{y1} + \Delta\delta_{y3}}{h}\right) \tag{7}$$

where h is the vertical distance between two TAAs. By the use of the small-angle approximation

$$\alpha = \frac{-\Delta\delta_{y1} + \Delta\delta_{y3}}{h}. \tag{8}$$

This approximation is valid, since the maximum value of the tilt angle is $\alpha = 0.17^{\circ}$, when the TAA hits upon the guide rail. The determination of β and γ occurs similarly. Finally, the transformation to global quantities writes

$$\mathbf{q} = \mathbf{T} \cdot \boldsymbol{\delta}_{\mathbf{sensor}} \tag{9}$$

where $\mathbf{T}$ is the transformation matrix

$$\mathbf{T} = \begin{bmatrix} 1/4 & 0 & -1/4 & 1/4 & 0 & -1/4 \\ 0 & 1/2 & 0 & 0 & 1/2 & 0 \\ 0 & -1/h & 0 & 0 & 1/h & 0 \\ 1/2h & 0 & -1/2h & -1/2h & 0 & 1/2h \\ -1/2b & 0 & -1/2b & -1/2b & 0 & -1/2b \end{bmatrix} \tag{10}$$

with b as the horizontal distance between two TAAs.

B. Force Transformation

The elevator car is assumed to behave like a rigid body. $\mathbf{M}$ is the symmetrical mass matrix, which contains the mass m and the moments of inertia I_x, I_y, and I_z of the elevator car

$$\mathbf{M} = \begin{pmatrix} m & 0 & 0 & 0 & 0 \\ 0 & m & 0 & 0 & 0 \\ 0 & 0 & I_x & 0 & 0 \\ 0 & 0 & 0 & I_y & 0 \\ 0 & 0 & 0 & 0 & I_z \end{pmatrix}. \tag{11}$$

Due to the small angular velocities and to the fact that there is no physical contact between the guide rail and elevator car, the bearing's damping and the Coriolis forces are neglected. The equation system reduces to

$$\mathbf{M}\ddot{\mathbf{q}}(t) = \mathbf{f}_{\mathbf{ext}}(\mathbf{t}) \tag{12}$$

with the vector of external forces $\mathbf{f}_{\mathbf{ext}}(\mathbf{t})$ acting on the elevator car.

To interact with the equation of motion, the local forces of the TAAs have also to be transformed to the vector of the global forces

$$\mathbf{F} = \mathbf{T}_{\mathbf{F}} \cdot \mathbf{f}_{\mathbf{local}} \tag{13}$$

where $\mathbf{f}_{\mathbf{local}}$ is the vector of the six control forces, shown in Fig. 6. $\mathbf{T}_{\mathbf{F}}$ is the force transformation matrix

$$\mathbf{T}_{\mathbf{F}} = \begin{bmatrix} 1 & 0 & -1 & 1 & 0 & -1 \\ 0 & 1 & 0 & 0 & 1 & 0 \\ 0 & -h/2 & 0 & 0 & h/2 & 0 \\ h/2 & 0 & -h/2 & -h/2 & 0 & h/2 \\ -b/2 & 0 & -b/2 & -b/2 & 0 & -b/2 \end{bmatrix}. \tag{14}$$

The transformation of the MMFs to global values is described in [17].

Authorized licensed use limited to: RWTH AACHEN. Downloaded on January 18, 2010 at 10:53 from IEEE Xplore. Restrictions apply.

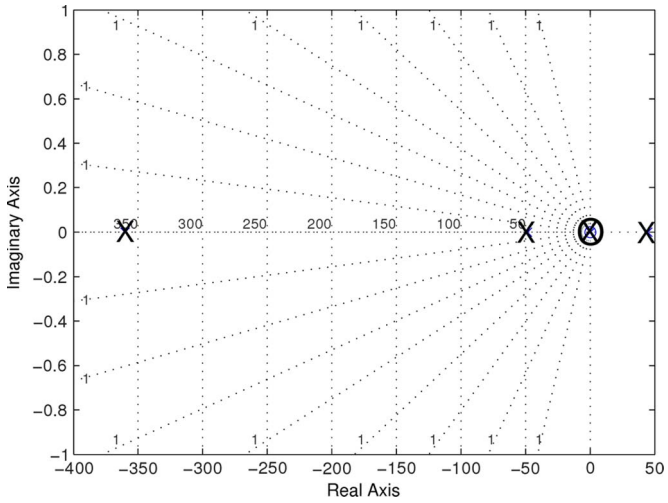

Fig. 8. Pole–zero plot of the uncontrolled DOF x.

C. Forming the State-Space Equation

The forming of the state-space equation for x, which is the first component of the position vector $\mathbf{q}$, is presented in this section. The procedure is similar for the other components.

Based on the mathematical modeling, the system description in state space is deduced from the governing differential equations. State variables are the spatial position x, velocity $\dot{x}$, and global MMF $\tilde{\Theta}_x$. In addition, the integral of the spatial position $\int x\,dt$ is added to the state vector to avoid a permanent deviation. After transforming the linearized force equations and the differential equation for current to global quantities [17], the state-space system is obtained

$$\underbrace{\begin{pmatrix} x \\ \dot{x} \\ \ddot{x} \\ \dot{\tilde{\Theta}}_x \end{pmatrix}}_{\dot{x}} = \underbrace{\begin{bmatrix} 0 & 1 & 0 & 0 \\ 0 & 0 & 1 & 0 \\ 0 & -\frac{4}{m}F_{\delta x} & 0 & \frac{8}{m}F_{\Theta x} \\ 0 & 0 & \Theta_{x0} & \Theta_{\Theta 0} \end{bmatrix}}_{A_x} \cdot \underbrace{\begin{pmatrix} \int x\,dt \\ x \\ \dot{x} \\ \tilde{\Theta}_x \end{pmatrix}}_{x} + \underbrace{\begin{bmatrix} 0 \\ 0 \\ 0 \\ U_0 \end{bmatrix}}_{B_x} \cdot \underbrace{(\tilde{U}_x)}_{u} \tag{15}$$

$$\mathbf{y} = \underbrace{(0 \quad 1 \quad 0 \quad 0)}_{C_x} \cdot \underbrace{\begin{pmatrix} \int x\,dt \\ x \\ \dot{x} \\ \tilde{\Theta}_x \end{pmatrix}}_{x}. \tag{16}$$

Here, $F_{\delta x}$, $F_{\Theta x}$, Θ_{x0}, $\Theta_{\Theta 0}$, and U_0 are the linearization factors. These two equations are the description of the uncontrolled system. A_x is the system matrix, B_x is the input matrix, and C_x is the output matrix. The feedthrough matrix D_x is chosen to be zero, since there is no direct feedthrough in a real system. Here, $\mathbf{y}$ is not the DOF y but the output vector of the state-space system. Fig. 8 shows the pole–zero plot of the uncontrolled DOF x, which depicts the eigenvalues of the system. It can be seen that not all poles are placed in the negative half-plane. Therewith, the system is unstable.

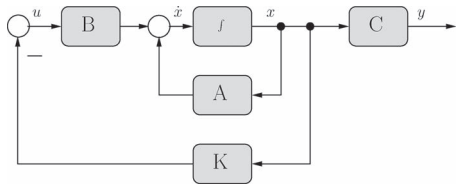

Fig. 9. Block-scheme representation of the state-space model.

IV. State Control

The control method employed is the so-called DOF control [18], [19]. A benefit of this method compared to a simple air-gap control [20], [21] (i.e., every single air-gap height is controlled separately) is a higher system stability, against the background of large manufacturing tolerances in high elevator shafts.

A. Controller Design

The entire DOF controller is designed with five parallel single-state controllers. The system matrix is formed, and with this, the state-space equation of the uncontrolled system is established. To stabilize the system, the poles of system matrix A_x have to be shifted. The eigenvalues are adjusted by a feedback of the state vector and a combination with the vector of the input values $\mathbf{u}$. Therefore, control matrix $\mathbf{K_x}$ is introduced. It contains the control parameters, one for each state variable. The controlled system is shown in Fig. 9 and described by the following:

$$\dot{\mathbf{x}} = \mathbf{A_x} \cdot \mathbf{x} + \mathbf{B_x} \cdot \mathbf{u}$$

$$\mathbf{u} = -\mathbf{K_x} \cdot \mathbf{x}. \tag{17}$$

Substituting the latter in the former results in

$$\mathbf{A_K} = \mathbf{A_x} - \mathbf{B_x} \cdot \mathbf{K_x} \tag{18}$$

with $\mathbf{A_K}$ as the system matrix of the controlled system.

In a further step, the control parameters are computed using the Riccati equation design rules [22]. These rules are based on a minimization of a squared control quality measure. For the control parameter optimization, the method of pole placement [22] is used. This method is presented in several publications. In [18] and [23], the use of this procedure is specified for the application in magnetic levitation controllers. Ghersin and Sánchez Peña [24] describe the pole placement for a 6-DOF vehicle. Other papers (e.g., [25]) show the implementation of the pole placement for other purposes. Finally, the pole–zero plot of the controlled system is obtained. It is shown in Fig. 10.

The controllers for the other four DOFs are established in the same way.

Authorized licensed use limited to: RWTH AACHEN. Downloaded on January 18, 2010 at 10:53 from IEEE Xplore. Restrictions apply.

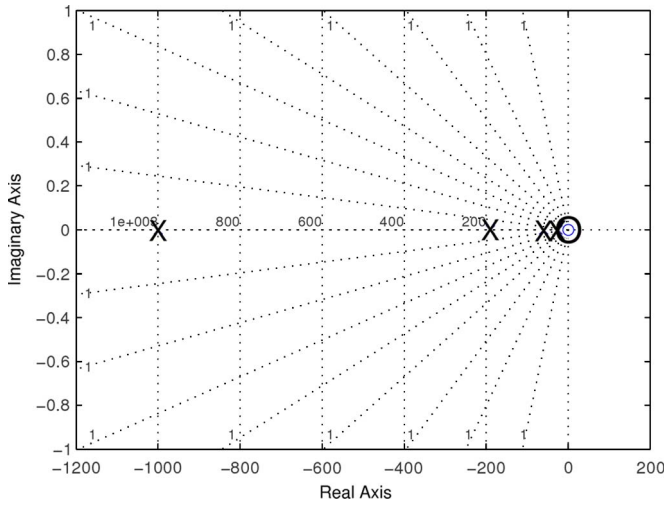

Fig. 10. Pole–zero plot of the controlled DOF x.

TABLE I
SIMULATED AND MEASURED VALUES FOR STIFFNESS OF ALL FIVE DOFS

DOF	minimum stiffness (simulation)	minimum stiffness (measurement)
x	$87.2\frac{N}{mm}$	$63.5\frac{N}{mm}$
y	$86.5\frac{N}{mm}$	$23\frac{N}{mm}$
α	$3.7\frac{kNm}{rad}$	$1.6\frac{kNm}{rad}$
β	$3.7\frac{kNm}{rad}$	$3.6\frac{kNm}{rad}$
γ	$3.0\frac{kNm}{rad}$	$2.0\frac{kNm}{rad}$

B. Simulation

In the first instance, the validity of the DOF control is verified by a dynamic simulation with Matlab/Simulink. Several realistic and worst case load cases are computed, as well as the stiffness of the guiding system. A couple of force impacts on different positions of the elevator car's walls and floor simulate the real load, i.e., walking and jumping individuals inside. The system response shows a robust guiding characteristic, even in extreme load cases [17]. For each DOF, the values for simulated and measured stiffness are compared in Table I.

C. Elevator Test Bench

The elevator test bench consists of an elevator shaft and an elevator car, operated with a rope. The sensor electronics and power converters of the guiding system are placed inside the elevator car. Each coil of the TAAs is driven by one dc/dc converter. The applied dc/dc converters are validated for the use as power electronics for electromagnets due to their former implementation in other magnetically levitated vehicles [18]. The elevator car is composed of an aluminum chassis, where the electronic devices are modularly integrated. Fig. 11 shows the front side of the elevator car inserted in the elevator shaft. The forefront of the plug-in units containing the dc/dc converters and the peripheral electronics can be seen in this figure.

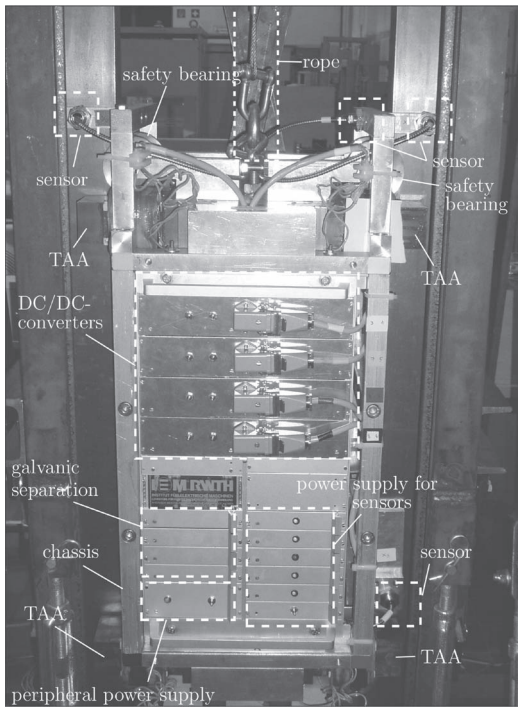

Fig. 11. Elevator car of the test bench.

The stiffness of the chassis is quite high; a deformation due to the electromagnetic forces of the actuating electromagnets is not expected. Hence, the measuring of five local positions is sufficient for a complete position estimation of the five DOFs. The actuators are mounted on two opposite edges of the roof and floor of the elevator car in a so-called symmetrical topology. The benefit of this topology is the low power consumption of the actuators since the uncontrolled suspension of the elevator car is in an unstable equilibrium when it is running without load.

Five position sensors are required to completely detect the position of the elevator car in the shaft. Therefore, five eddy-current sensors are mounted on the linear guiding system to measure the distance between the actuators and their return yokes. The complete block-scheme representation of the test bench can be seen in Fig. 12. The signal flow from the position vector $\mathbf{q}$ to the vector of magnetic forces $\mathbf{f_m}$ is presented. Air-gap heights are measured with eddy-current sensors. Then, the analog signal is filtered by a low-pass filter for antialiasing. After A/D transformation, the designed control algorithm is used. The signal is transformed back by a D/A transformation. A galvanic separation between the control and power part of the test bench is ensured by using an optocoupler. The reference voltage is the input signal for the current controllers of the dc/dc converters. The output currents drive the coils of the actuators. Finally, electromagnetic forces act on the elevator car. The feedback of the position vector $\mathbf{q}$ symbolizes the dependence of the electromagnetic force from the air-gap height.

1) Force Impulse: The spatial displacement of the elevator car resulting from a force impulse of 100 N in the x-direction is shown in Fig. 13. After a short oscillation with a maximum displacement of 0.09 mm, the system returns to the working

Authorized licensed use limited to: RWTH AACHEN. Downloaded on January 18, 2010 at 10:53 from IEEE Xplore. Restrictions apply.

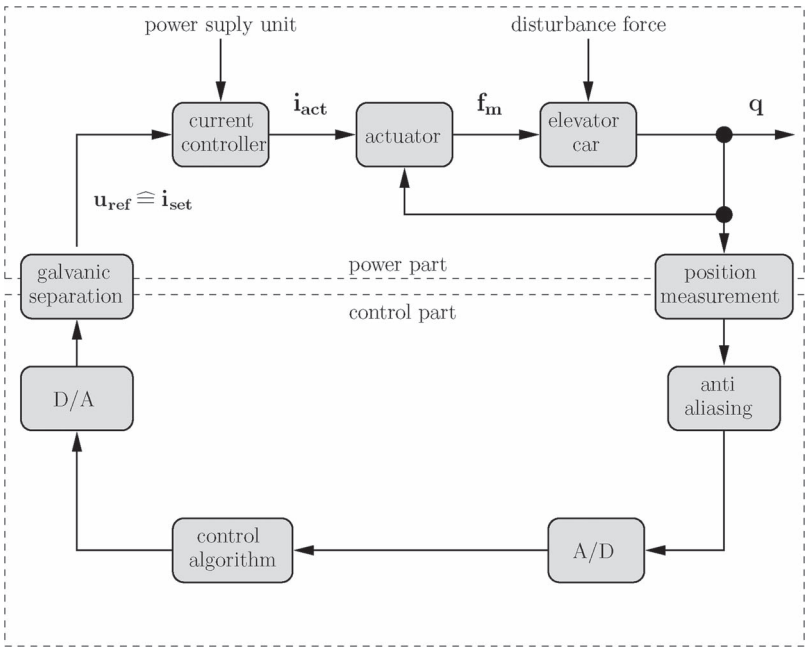

Fig. 12. Block-scheme representation of the full system.

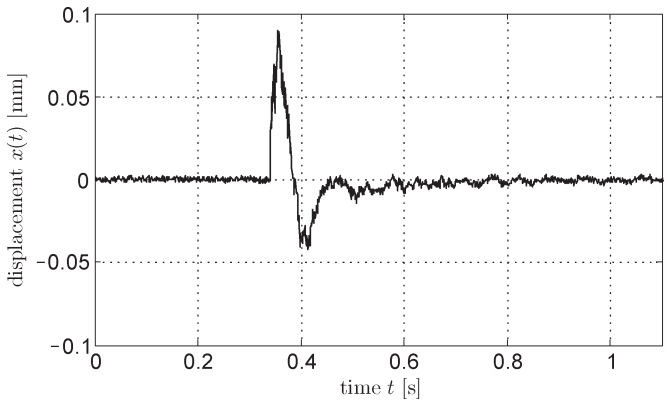

Fig. 13. Position error of the controlled system in the x-direction.

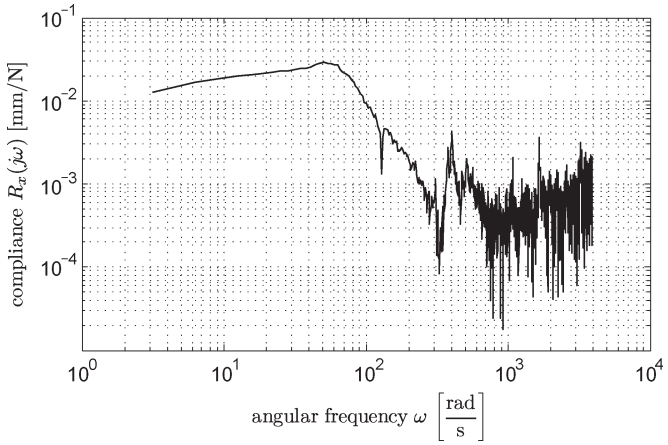

Fig. 14. Compliance of the controlled system in the x-direction.

point $\mathbf{q_0}$. Fig. 14 shows the compliance characteristic of the DOF x. It can be seen that the maximum compliance occurs at an angular frequency of $\omega \approx 60(1/s)$. The reciprocal value of the maximum compliance is the minimum stiffness. This is a common quantity for the comparison of magnetically levitated vehicles. In Table I, the minimum stiffness for all components of the spatial position vector $\mathbf{q}$ is specified. Simulation and measurements match regarding DOF x, β, and γ. Only y and α strongly deviate. These two DOFs are excited by the forces resulting from the central arms of the TAAs. Simplifications in the modeling process like neglecting the permeability of the iron yoke lead to major deviations between simulation and measurement. The improvement of the stiffness of these DOFs is a current field of research.

2) Air-Gap Variations: The displacement of the guide rails resulting from oscillations in very high buildings leads to variations of the air-gap length. Hereby, the reluctances of the local air gaps vary. Nonetheless, a sufficient operation of the linear guiding system must be ensured. For testing purposes, three thin steel plates are attached on top of each other to one guide rail in the y-direction, so that the air gap decreases to 2.5 mm in this area. Fig. 15 shows the DOF during a transit through the surface defect. Small deviations from the equilibrium can be seen as the elevator car passes the defect area. The displacement occurs in the affected DOFs y and α. In spite of leaving the working point $\mathbf{q_0}$, the elevator car does not collide with the guide rail. Thus, the functionality of the control system is proven.

3) Input Power: The input power of the linear guiding system with offline control is $P_{\text{off}} = 25$ W. This power is mainly used for the supply of the eight dc/dc converters of the actuator windings (Fig. 11). The input power during dynamic operation is shown in Fig. 16. The base load is $P_{\text{base}} \approx 55$ W. The four power peaks in the diagram are due to sudden load changes on the elevator car. It can be seen that the highest power demand of $P_{\max} \approx 110$ W is required for a short period of time only. The energy balance of the guiding system is hardly affected.

Authorized licensed use limited to: RWTH AACHEN. Downloaded on January 18, 2010 at 10:53 from IEEE Xplore. Restrictions apply.

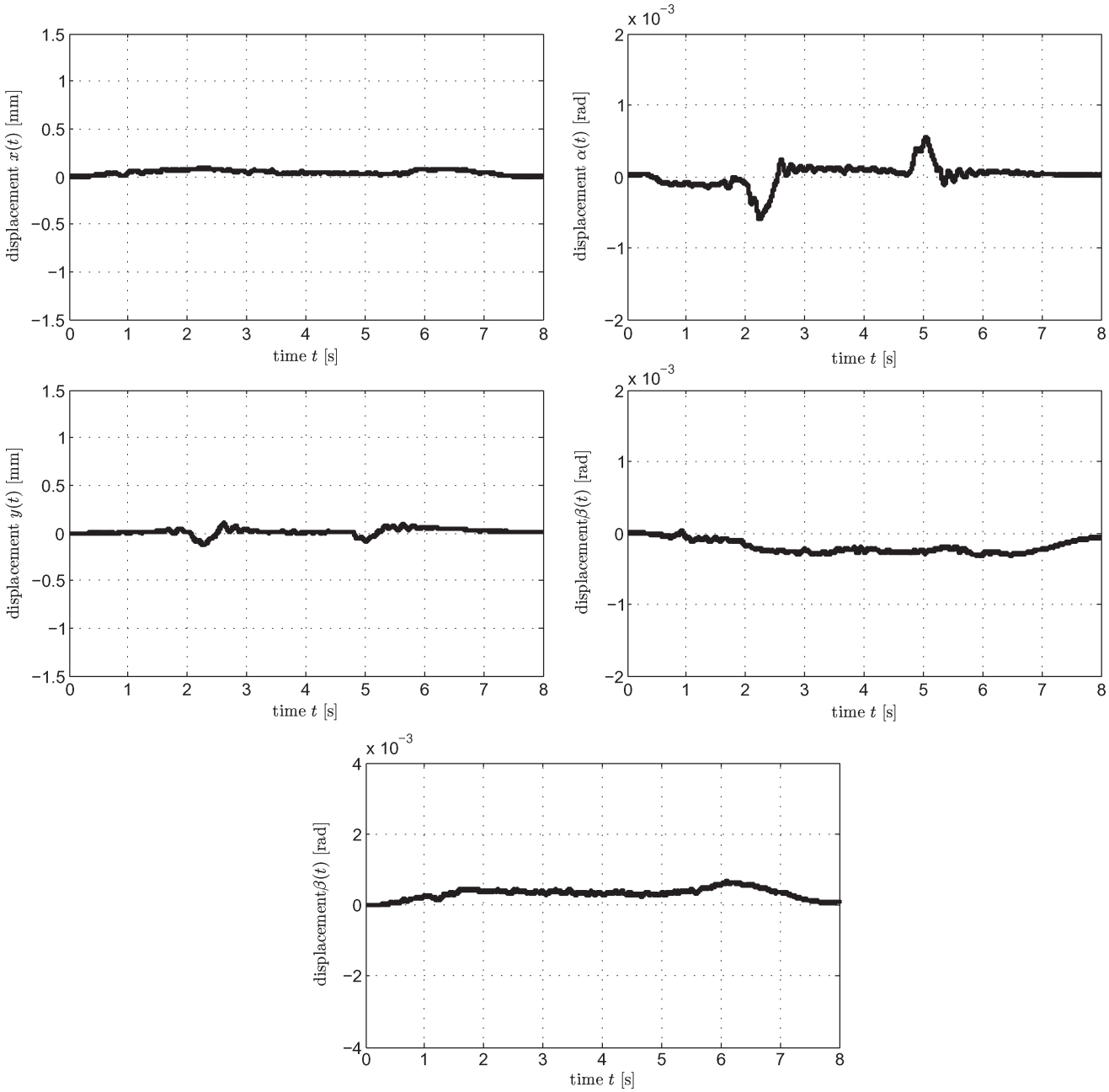

Fig. 15. Transit through areas with reduced air gaps in the y-direction.

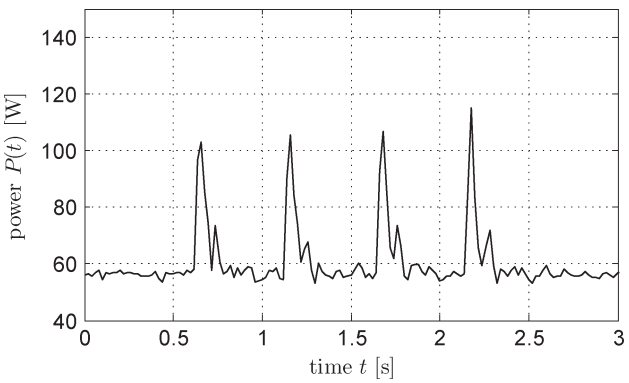

Fig. 16. Input power of the linear guiding system at dynamic operation.

V. Conclusion

Several load cases have been simulated and tested with the elevator test bench. The results show a robust state-space controller with a high control quality. The topology of this guiding system and its advantages are introduced in the beginning. The functionality of the TAA is explained in detail. Thereafter, it is indicated that the system of four TAA actuators is overdetermined. Experimental results are presented, which validate the functionality of the system. Neglecting saturation and eddy-current losses in the MEC approach yields a small divergence between measurement results and theory. Further improvement in these areas is needed to increase the accuracy of the modeling process.

Authorized licensed use limited to: RWTH AACHEN. Downloaded on January 18, 2010 at 10:53 from IEEE Xplore. Restrictions apply.

REFERENCES

[1] M. Platen and G. Henneberger, "Examination of leakage and end effects in a linear synchronous motor for vertical transportation by means of finite element computation," *IEEE Trans. Magn.*, vol. 37, no. 5, pp. 3640–3643, Sep. 2001.

[2] H. S. Lim, R. Krishnan, and N. S. Lobo, "Design and control of a linear propulsion system for an elevator using linear switched reluctance motor drives," *IEEE Trans. Ind. Electron.*, vol. 55, no. 2, pp. 534–542, Feb. 2008.

[3] H. S. Lim and R. Krishnan, "Ropeless elevator with linear switched reluctance motor drive actuation systems," *IEEE Trans. Ind. Electron.*, vol. 54, no. 4, pp. 2209–2218, Aug. 2007.

[4] N. S. Lobo, H. S. Lim, and R. Krishnan, "Comparison of linear switched reluctance machines for vertical propulsion application: Analysis, design, and experimental correlation," *IEEE Trans. Ind. Appl.*, vol. 44, no. 4, pp. 1134–1142, Jul./Aug. 2008.

[5] J. Batelaan, "A linear motor design provides close and secure vehicle separation of many transit vehicles on a guideway," *IEEE Trans. Ind. Electron.*, vol. 54, no. 3, pp. 1778–1782, Jun. 2007.

[6] S.-M. Yang and M.-S. Huang, "Design and implementation of a magnetically levitated single-axis controlled axial blood pump," *IEEE Trans. Ind. Electron.*, vol. 56, no. 6, pp. 2213–2219, Jun. 2009.

[7] Z. V. Despotovic and Z. Stojiljkovic, "Power converter control circuits for two-mass vibratory conveying system with electromagnetic drive: Simulations and experimental results," *IEEE Trans. Ind. Electron.*, vol. 54, no. 1, pp. 453–466, Feb. 2007.

[8] C. K. Lim, I.-M. Chen, L. Yan, G. Yang, and K.-M. Lee, "Electromechanical modeling of a permanent-magnet spherical actuator based on magnetic-dipole-moment principle," *IEEE Trans. Ind. Electron.*, vol. 56, no. 5, pp. 1640–1648, May 2009.

[9] J. Sallan, J. L. Villa, A. Llombart, and J. F. Sanz, "Optimal design of ICPT systems applied to electric vehicle battery charge," *IEEE Trans. Ind. Electron.*, vol. 56, no. 6, pp. 2140–2149, Jun. 2009.

[10] G. Covic, J. Boys, M. Kissin, and H. Lu, "A three-phase inductive power transfer system for roadway-powered vehicles," *IEEE Trans. Ind. Electron.*, vol. 54, no. 6, pp. 3370–3378, Dec. 2007.

[11] J.-Y. Chen, J.-B. Zhou, G. Meng, and W.-M. Zhang, "Evaluation of eddy-current effects on diamagnetic bearings for microsystems," *IEEE Trans. Ind. Electron.*, vol. 56, no. 4, pp. 964–972, Apr. 2009.

[12] M. Morishita and M. Akashi, "Electromagnetic non-contact guide system for elevator cars," in *Proc. 3rd Int. Symp. LDIA*, Nagano, Japan, Oct. 2001, pp. 416–419.

[13] M.-Y. Chen, M.-J. Wang, and L.-C. Fu, "Modeling and controller design of a maglev guiding system for application in precision positioning," *IEEE Trans. Ind. Electron.*, vol. 50, no. 3, pp. 493–506, Jun. 2003.

[14] T. Tsuji, K. Ohnishi, and A. Sabanovic, "A controller design method based on functionality," *IEEE Trans. Ind. Electron.*, vol. 54, no. 6, pp. 3335–3343, Dec. 2007.

[15] B. Schmülling, O. Effing, and K. Hameyer, "State control of an electromagnetic guiding system for ropeless elevators," in *Proc. EPE*, Aalborg, Denmark, Sep. 2007, pp. 1–10.

[16] A. Schmidt, C. Brecher, and F. Possel-Dölken, "Novel linear magnetic bearings for feed axes with direct drives," in *Proc. Int. Conf. Smart Mach. Syst. Nat. Inst. Stand. Technol.*, Gaithersburg, MD, Mar. 2007, pp. 427–432.

[17] B. Schmülling, R. Appunn, and K. Hameyer, "Electromagnetic guiding of vertical transportation vehicles: State control of an over-determined system," in *Proc. XVIII ICEM*, Vilamoura, Portugal, Sep. 2008, pp. 1–6.

[18] J. Van Goethem and G. Henneberger, "Design and implementation of a levitation-controller for a magnetic levitation conveyor vehicle," in *Proc. 8th Int. Symp. Magn. Bear.*, Mito, Japan, Aug. 2002, pp. 139–142.

[19] D. Li and H. Gutierrez, "Observer-based sliding mode control of a 6-DOF precision maglev positioning stage," in *Proc. 34th IEEE IECON*, Orlando, FL, Nov. 2008, pp. 2562–2567.

[20] D. Li and H. Gutierrez, "Precise motion control of a hybrid magnetic suspension actuator with large travel," in *Proc. 34th IEEE IECON*, Orlando, FL, Nov. 2008, pp. 2661–2666.

[21] A. Forrai, T. Ueda, and T. Yumura, "Electromagnetic actuator control: A linear parameter-varying (LPV) approach," *IEEE Trans. Ind. Electron.*, vol. 54, no. 3, pp. 1430–1441, Jun. 2007.

[22] O. Föllinger, *Regelungstechnik—Einführung in die Methoden und ihre Anwendung*, 8th ed. Braunschweig, Germany: Hüthig Buch Verlag Heidelberg, 1994.

[23] Y. S. Lu and J. S. Chen, "Design of a perturbation estimator using the theory of variable-structure systems and its application to magnetic levitation systems," *IEEE Trans. Ind. Electron.*, vol. 42, no. 3, pp. 281–289, Jun. 1995.

[24] A. S. Ghersin and R. S. Sánchez Peña, "LPV control of a 6-DOF vehicle," *IEEE Trans. Control Syst. Technol.*, vol. 10, no. 6, pp. 883–887, Nov. 2002.

[25] A. R. Oliva, S. S. Ang, and G. E. Bortolotto, "Digital control of a voltage-mode synchronous buck converter," *IEEE Trans. Power Electron.*, vol. 21, no. 1, pp. 157–163, Jan. 2006.

Rüdiger Appunn received the M.Sc. degree in electrical engineering from the Faculty of Electrical Engineering and Information Technology, RWTH Aachen University, Aachen, Germany, in 2008.

Since 2008, he has been a Researcher at the Institute of Electrical Machines, RWTH Aachen University. His research fields include magnetic levitation, mechatronics, and control.

Benedikt Schmülling received the M.Sc. degree in electrical engineering from the Faculty of Electrical Engineering and Information Technology, University of Dortmund, Dortmund, Germany, in 2005, where he was also working as an Engineer.

Since 2005, he has been a Researcher at the Institute of Electrical Machines, RWTH Aachen University, Aachen, Germany. His research fields include magnetic levitation, mechatronics, and control.

Kay Hameyer (M'96–SM'99) received the M.Sc. degree in electrical engineering from the University of Hannover, Hannover, Germany, and the Ph.D. degree from the University of Technology Berlin, Berlin, Germany.

After his university studies, he was with Robert Bosch GmbH, Stuttgart, Germany, as a Design Engineer for permanent-magnet servomotors and electrical energy-supply system components. In 1988, he was a Member of the Staff at the University of Technology Berlin. He was a Full Professor of numerical field computations and electrical machines at the Katholieke Universiteit Leuven, Leuven, Belgium, until February 2004. In 2005, he was with Poznan University of Technology, Poznan, Poland. He is currently a Full Professor, the Director of the Institute of Electrical Machines, and the holder of the Chair "Electromagnetic Energy Conversion" at RWTH Aachen University, Aachen, Germany, where he has also been the Dean of the Faculty of Electrical Engineering and Information Technology since 2007. His research interests include numerical field computation and simulation, design of electrical machines, particularly permanent-magnet excited machines and induction machines, and numerical optimization strategies.

Authorized licensed use limited to: RWTH AACHEN. Downloaded on January 18, 2010 at 10:53 from IEEE Xplore. Restrictions apply.